MIT Open Access Articles

A CHANDRA OBSERVATION OF 3C 288— REHEATING THE COOL CORE OF A 3 keV CLUSTER FROM A NUCLEAR OUTBURST at z = 0.246

Massachusetts Institute of Technology

A *CHANDRA* OBSERVATION OF 3C 288—REHEATING THE COOL CORE OF A 3 keV CLUSTER FROM A NUCLEAR OUTBURST at $z = 0.246$

D. V. Lal[1], R. P. Kraft[1], W. R. Forman[1], M. J. Hardcastle[2], C. Jones[1], P. E. J. Nulsen[1], D. A. Evans[1,3],
J. H. Croston[4], and J. C. Lee[1]
[1] Harvard-Smithsonian Center for Astrophysics, 60 Garden Street, Cambridge, MA 02138, USA
[2] School of Physics, Astronomy, and Mathematics, University of Hertfordshire, Hatfield, AL 10 9AB, UK
[3] MIT Kavli Institute for Astrophysics and Space Research, 77 Massachusetts Avenue, Cambridge, MA 02139, USA
[4] School of Physics and Astronomy, University of Southampton, Southampton, SO17 1SJ, UK

ABSTRACT

We present results from a 42 ks *Chandra*/ACIS-S observation of the transitional FR I/FR II radio galaxy 3C 288 at $z = 0.246$. We detect ∼3 keV gas extending to a radius of ∼0.5 Mpc with a 0.5–2.0 keV luminosity of 6.6×10^{43} erg s^{-1}, implying that 3C 288 lies at the center of a poor cluster. We find multiple surface brightness discontinuities in the gas indicative of either a shock driven by the inflation of the radio lobes or a recent merger event. The temperature across the discontinuities is roughly constant with no signature of a cool core, thus disfavoring either the merger cold front or sloshing scenarios. We argue therefore that the discontinuities are shocks due to the supersonic inflation of the radio lobes. If they are shocks, the energy of the outburst is ∼10^{60} erg, or roughly 30% of the thermal energy of the gas within the radius of the shock, assuming that the shocks are part of a front produced by a single outburst. The cooling time of the gas is ∼10^8 yr, so that the energy deposited by the nuclear outburst could have reheated and efficiently disrupted a cool core.

Key words: galaxies: individual (3C 288) – galaxies: jets – hydrodynamics – intergalactic medium – X-rays: galaxies: clusters

Online-only material: color figures

1. INTRODUCTION

Chandra has revolutionized our knowledge of the energetic processes involved in the jets, the lobes, and the nuclei of radio galaxies. The X-ray images of the hot atmospheres in galaxies show a wealth of structures associated with central radio sources, including cavities, metal enriched plumes, filaments, and shock fronts (Peterson & Fabian 2006; McNamara & Nulsen 2007; McNamara et al. 2009). High-resolution spectroscopic observations from *Chandra* and *XMM-Newton* have conclusively ruled out simple, steady cooling flow models, and this has been one of the significant discoveries (Peterson & Fabian 2006; David et al. 2006). Since the cooling time of gas in many cluster cores is much less than the Hubble time, energy must be occasionally or continuously supplied to cluster cores to prevent the formation of cooling flows. A primary candidate for the suppression of cluster cooling flows is feedback between the central supermassive black hole (SMBH) of active galaxy and the cluster gas.

Studies of the X-ray gas environments of FR I and FR II sources with *Chandra* have led to important new constraints on how jets propagate through their ambient media, and how radio lobes interact with and transfer energy to their large-scale gas environments (e.g., Hardcastle et al. 2002; Sambruna et al. 2004; Kraft et al. 2006). However, "high-excitation" FR II sources tend to lie in low gas mass atmospheres at least at low redshifts (Ellingson et al. 1991a, 1991b, 1991c; Harvanek et al. 2001, 2002; Isobe et al. 2005; Kraft et al. 2007), unless the mechanical power of the jet is unusually high (e.g., Cygnus A; Smith et al. 2002). This strongly suggests that the jet power and the interaction between jets and the hot gas in their vicinity play pivotal roles in governing the overall morphology (FR I versus FR II) of the radio source.

The radio source 3C 288 is identified with an elliptical galaxy with $m_v = 18.3$ ($M_v = -22.08$; Goodson et al. 1979). It is the archetypal example of a transitional FR I/FR II ("jetted double") radio galaxy (Fanaroff & Riley 1974). In optical imaging, there are fainter galaxies in the field which are presumed to be members of a cluster that is dominated by 3C 288 (Wyndham 1966). Dominant cluster members can produce asymmetric "wide-angle-tail" (WAT) radio structures (Burns et al. 1986), despite their presumed low peculiar velocities, but 3C 288 is not a clear example of WAT morphology. Its monochromatic power at 1.5 GHz is 2.5×10^{33} erg s^{-1} Hz^{-1} and its integrated spectral index $\alpha_{0.75}^{5.0}$ between 0.75 GHz and 5.0 GHz is -0.97 (Laing & Peacock 1980; $s_\nu \propto \nu^\alpha$). Its radio luminosity would place it firmly in the high-power (i.e., FR II) regime, and yet its observational characteristics, in particular its edge-darkened radio morphology, are strikingly different from those of the canonical "classical double" radio galaxies. Although the edge darkening of the radio structure and its spectral distribution are reminiscent of a (distorted) radio "trail," no other properties of 3C 288 suggest that it belongs to this morphological class. The structure of 3C 288 is more asymmetric than those of normal double sources of its size and radio power (Bridle et al. 1989). Very Large Array (VLA) observations reveal a jet and a counterjet near the radio core, and faint "wings" of emission connected to the elongated lobes (Bridle et al. 1989). The small radio size, unusual morphology, and polarization asymmetries of 3C 288 raise the possibility that it is interacting strongly with the ambient gas (Bridle et al. 1989). Thus, 3C 288 is an ideal candidate for study with *Chandra* to better understand the role that active galactic nucleus (AGN) heating may play in the formation of radio structure in the hot phase of the intergalactic medium (IGM).

This paper is organized as follows. Section 2 contains a summary of the observational details. Results of the data analysis are presented in Section 3 and we discuss their implications in Section 4. Section 5 contains a brief summary
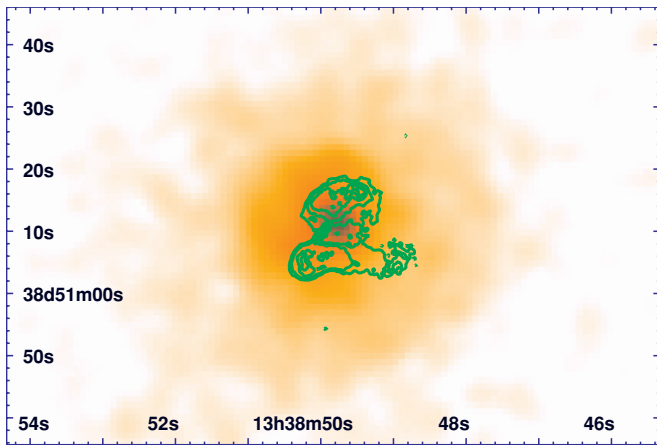
Figure 1. Gaussian-smoothed (radius$_{FWHM}$ = 2″), exposure-corrected, background-subtracted *Chandra*/ACIS-S image of 3C 288 in the 0.5–2.5 keV band. All point sources, other than the active nucleus of 3C 288, have been removed. We see diffuse thermal emission with a temperature of ~3 keV extending to ~510 kpc (~1′.73). Contours from the 4.9 GHz radio map of 3C 288 are overlaid and 10 contour levels are placed linearly between 0.4 and 12.0 mJy beam^{-1}. The radio source is small, 294 kpc (1′.3 across), and the radio core is coincident with the optical host galaxy. A peak of X-ray emission lies ~11.2 kpc (~3′′.0) east of the optical host galaxy.

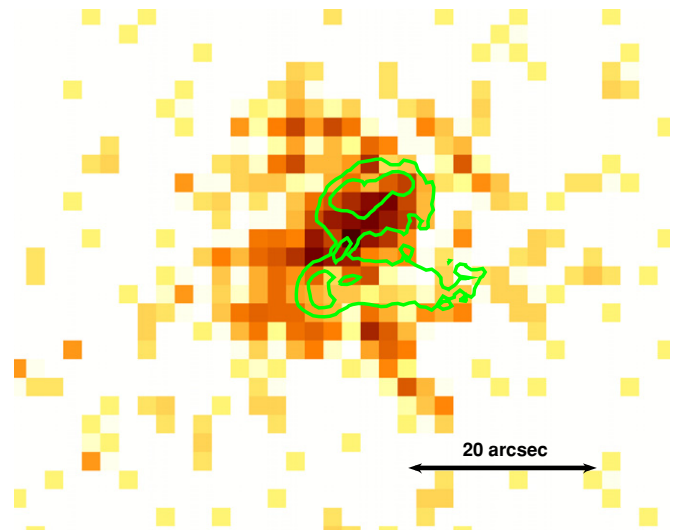(A color version of this figure is available in the online journal.)

Figure 2. *Chandra*/ACIS-S image of 3C 288 in the 0.23–0.50 keV soft X-ray band with 5 GHz radio contours (0″.6 resolution) overlaid. This image shows the soft X-ray excess, which is not commonly observed in clusters of galaxies and is uniformly detected across the whole 42 ks observation.

(A color version of this figure is available in the online journal.)

and conclusions. We assume *Wilkinson Microwave Anisotropy Probe* cosmology throughout this paper (Spergel et al. 2007). The observed redshift ($z = 0.246$) of the host galaxy of 3C 288 corresponds to a luminosity distance of 1192.9 Mpc, and 1″ = 3.725 kpc. All coordinates are J2000. The elemental abundances are relative to the solar value tabulated by Anders & Grevasse (1989). Absorption by gas in our galaxy ($N_H = 9 \times 10^{19}$ cm^{-2}, Dickey & Lockman 1990) is included in all our spectral fits.

2. OBSERVATIONS

The radio galaxy 3C 288 was observed on 2008 April 13 (ObsID: 9275; PI: D.A. Evans) with *Chandra*/ACIS-S in VFAINT mode for ~42.0 ks. We made light curves for each CCD in the 0.5–10.0 keV band in order to search for background flares and intervals where the background rate was high; none were present, leaving 39647.8 s of good data. We performed the usual filtering by grade, excluded bad/hot pixels and columns, removed cosmic-ray "afterglows," and applied the VF mode filtering using tools built in CIAO (http://cxc.harvard.edu/ciao). Images were generated after subtracting background and correcting for exposure (which included all the effects mentioned above).

We use archival VLA observations of 3C 288 at 4.885 GHz (Bridle et al. 1989). The map is taken from the online 3CRR Atlas[5] which provides well-calibrated, well-sampled images.

3. DATA ANALYSIS

A Gaussian-smoothed (radius$_{FWHM}$ = 2″) *Chandra*/ACIS-S image of 3C 288 in the 0.23–5.00 keV band with radio contours overlaid is shown in Figure 1. All point sources other than the 3C 288 nucleus have been removed. We detect diffuse thermal emission from the cluster intracluster medium (ICM) with a temperature of ~3 keV extending to ~390 kpc (~104″). Diffuse

emission from the source fills only a fraction (~3%) of the area in the S3-chip, so local background was extracted for all spectral analyses, from the source-free region on the S3 chip. The radio source is small, ~67.1 kpc (= 18″ across), and the X-ray bright gas core lies ≃11.2 kpc (~3″) north of the radio core; this offset is perhaps associated with the non-hydrostatic motion of the gas. The X-ray isophotes within 112 kpc (0′.5) of the nucleus are circular. For simplicity we assume spherical symmetry in our analysis below. On larger scales, however, the isophotes show an extension to the southeast.

Interestingly, we detect significant X-ray emission below 0.50 keV. Such emission is not commonly observed in clusters of galaxies with *Chandra*, and was initially suggestive of inverse Compton scattering of cosmic microwave background photons from a large population of cosmic-ray electrons in the cluster core, similar to that claimed for the Coma cluster (Sarazin & Lieu 1998; Finoguenov et al. 2003; Erlund et al. 2007). This emission lies predominantly at the cluster core. Additionally, it appears that there is a cavity in the gas associated with the southern radio lobe and that the 0.23–0.50 keV emission is roughly aligned with the jet axis. However, there is no obvious direct correspondence between this soft X-ray emission and radio features as seen in Hydra A (Nulsen et al. 2005). An image of the cluster in the 0.23–0.50 keV band with radio contours overlaid is shown in Figure 2. We created surface brightness profiles of the emission in the 0.3–0.5 keV (soft) and 0.5–1.5 keV (hard) bands, subtracted an appropriate background, and fitted a line to the ratio of soft and hard X-ray emission as a function of distance from the center. The slope of this line is consistent with zero within the uncertainties and we confirm that, within the statistical uncertainties, there is no difference in the spatial distribution of this soft X-ray emission relative to the hard X-ray emission. Spectral analysis of the *Chandra* data, combined with spectral analysis of archival *ROSAT* PSPC data, confirms that this emission is simply the bremsstrahlung continuum emission from an ~3 keV plasma. It is only visible in the 3C 288 cluster because of the combination of gas temperature and unusually low Galactic column.

---

[5] ATLAS catalog: radio images and other data for the nearest 85 DRAGNs (radio galaxies and related objects) in the so-called 3CRR sample of Laing et al. (1983). Available at http://www.jb.man.ac.uk/atlas/index.html.

3.1. Compact Components

Contours from the 4.9 GHz radio map of 3C 288 are shown in Figure 1 overlaid on the background-subtracted, exposure-corrected, Gaussian-smoothed *Chandra* ACIS-S image. The core is the brightest, most compact radio feature (Bridle et al. 1989), and coincides with the optical position of the nucleus (Goodson et al. 1979). It has a flux density, $S_{4.9\,GHz}$, of 12.68 ± 0.07 mJy (1 mJy $= 10^{-26}$ erg s^{-1} cm^{-2} Hz^{-1}). The northern and southern hot spots are clearly detected in the 4.9 GHz and 1.4 GHz radio maps and have flux densities of 6.88 ± 0.09 mJy and 5.84 ± 0.11 mJy, respectively, at 4.9 GHz. The radio core has a spectral index of $\alpha_{1.4\,GHz}^{5.0\,GHz} = -0.76 \pm 0.02$ ($s_\nu \propto \nu^\alpha$, where S_ν is the flux density at frequency ν and the error bars are 1σ confidence). The northern and southern hot spots have spectral indices of $\alpha_{1.4\,GHz}^{5.0\,GHz} = -0.76 \pm 0.04$ and -0.87 ± 0.06, respectively. We do not detect an X-ray point source (see Figure 1) at the location of the radio core. Only eight net counts above the background were extracted in a $0\farcs5$ radius circle at the location of the core with no point source evident above the level of the diffuse emission from the gas. The 3σ upper limit to the 1 keV (rest frame) flux density of the core is ~ 0.31 nJy assuming a photon index of 2 and Galactic absorption. Assuming that this upper limit represents non-thermal X-rays from the AGN, the upper limit to the radio to X-ray power-law index is $\alpha_{\rm radio}^{\rm X-ray} \simeq -0.99 \pm 0.02$. The corresponding core radio luminosity at 178 MHz assuming a flat spectrum and the unabsorbed core X-ray luminosity at 1 keV are consistent with the expectation from the correlation between these two quantities shown in Hardcastle et al. (2009).

No X-ray emission is detected from the jet or the compact hot spots of the two lobes. With no point source evident and zero counts above the diffuse emission from the gas, we use the 3σ counts of seven, by measuring the off-source background level and then use Poisson statistics to find the number of counts corresponding to a 3σ Gaussian probability, for the northern and the southern hot spots. The 3σ upper limit to the 1 keV (rest-frame) flux density of both the northern and southern hot spots is ~ 0.29 nJy assuming a photon index of 2 and Galactic absorption. We deduce upper limits to the X-ray–radio power-law indices for the northern and southern hot spots of $\alpha_{\rm radio}^{\rm X-ray} \gtrsim -0.96 \pm 0.02$ and $\gtrsim -0.95 \pm 0.02$, respectively (again, the error bars are at 1σ confidence). If we use these spectral indices, the expected flux densities in the optical and infrared bands, $S_{5000\,\textrm{Å}}$ and $S_{7\,\mu}$ are 0.09 and 1.15 μJy for the northern hot spot, and 0.09 and 1.07 μJy for the southern hot spot, respectively. These are undetectable with the current generation of optical and infrared observatories. There is no non-thermal emission detected from the nucleus, lobes, or jets from this radio galaxy, and the upper limits are consistent with detections of such emission in much closer radio galaxies.

3.2. Large-scale Diffuse X-ray Emission

The extended, diffuse X-ray emission seen in Figure 1 is attributed to emission from the hot gas of a cluster atmosphere. We derived a global temperature and metallicity for 3C 288 within a $1'$ radius circular region covering the majority of the cluster emission. The spectrum was extracted using the CIAO[6] specextract tool, binned to 10 counts per bin and fitted in the 0.5–5.0 keV range using an absorbed APEC model within

---

[6] All spectral extraction and spectral analysis were performed using CIAO v4.1, the CALDB v4, and XSPEC v12.5.1.
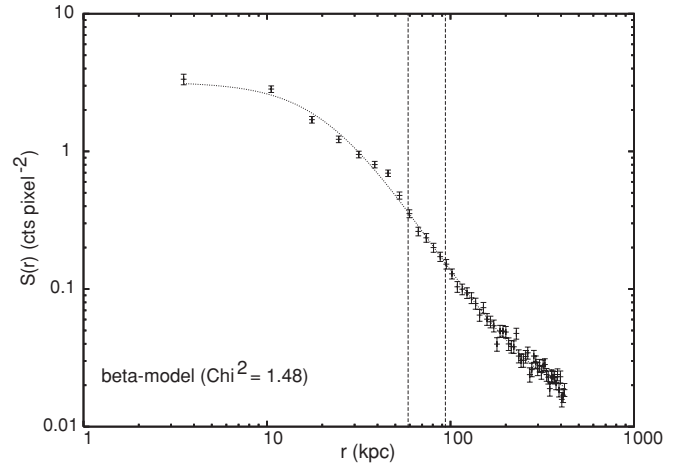

Figure 3. Azimuthally averaged radial surface brightness profile of the X-ray emission from the gas in the energy band from 0.5 keV to 2.5 keV. The best-fit isothermal β-model profile has been overlaid. The two vertical lines show the location of prominent, sharp edges in X-ray brightness at distances from the nucleus of 53.3 kpc ($14\farcs2$) and 91.1 kpc ($24\farcs4$) along the eastern and the southwestern directions, respectively.

the XSPEC package (Arnaud 1996). The neutral hydrogen column density was fixed at the Galactic foreground value of $N_{\rm H} = 9.0 \times 10^{19}$ cm^{-2}. The best-fitting values for temperature and abundance are $k_B T = 2.94_{+0.19}^{-0.18}$ keV and $Z = 0.73_{-0.19}^{+0.16}$, respectively, where the errors are 90% confidence limits. If we allow the neutral hydrogen column density to be a free parameter, the best-fitting values for temperature and abundance do not change appreciably, and the changes are smaller than 1σ uncertainties. The unabsorbed X-ray luminosity from the best-fitting model in the energy range 0.5–5.0 keV is $(1.11 \pm 0.03) \times 10^{44}$ erg s^{-1} within the $r = 223.5$ kpc ($1'$) circular aperture. Additionally, the unabsorbed X-ray luminosity in the energy range 0.5–2.4 keV is $(7.60 \pm 0.18) \times 10^{43}$ erg s^{-1} and the result is consistent with the expectations for a 3 keV cluster (Markevitch 1998). The azimuthally averaged radial surface brightness profile of the X-ray emission from the gas is shown in Figure 3. The best-fitting isothermal β-model profile has been overlaid. We find $\beta = 0.52 \pm 0.02$ and a core radius $r_0 = 11\farcs94 \pm 0\farcs93$ from fitting the surface brightness profile between $3''$ and $200''$ from the nucleus.

We find two breaks in the surface brightness distribution, one $14\farcs2$ east of the nucleus and another $24\farcs4$ to the southwest, as shown by the black arrows in Figure 4. The presence of these breaks in the surface brightness distribution implies a sharp change in the gas density or temperature of the gas across the discontinuities. *Chandra* has observed a large number of similar features in other clusters, such as A1795 (Markevitch et al. 2001), A3667 (Vikhlinin et al. 2001b), M87 (Forman et al. 2005, 2007), Hydra A (Nulsen et al. 2005), MS 0735.6+7421 (McNamara et al. 2005), and A1201 (Owers et al. 2009), and they are generally attributed to three phenomena: merger cold fronts, sloshing of cluster cores due to non-hydrostatic motions of the gas, and shocks due to nuclear outbursts. Most merger cold fronts are offset from the center (e.g., A3667) and are the result of the infall of a massive subclump into the cluster. Unless we are viewing such a merger head-on, the morphology of these features in the 3C 288 cluster gas is very different than what we observe in A3667 (Vikhlinin et al. 2001b). Additionally, it would be surprising, if we are witnessing a major merger from such a viewing angle, if the cluster lies on the L_x–T relation.
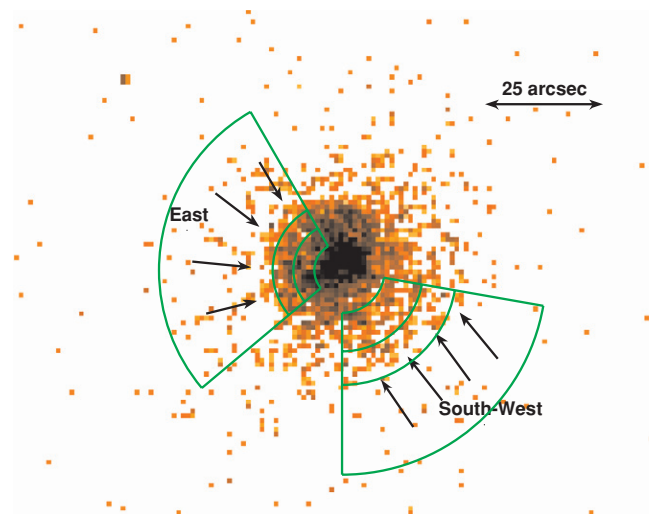
Figure 4. Gaussian-smoothed (radius$_{\text{FWHM}} = 2''$) *Chandra*/ACIS-S image in the 0.23–2.50 keV band. The image has $2''$ bins. The black sets of arrows denote the positions of two surface brightness discontinuities. The image also shows regions where surface brightness profiles were fitted and where spectra were extracted for temperature measurements. A large $1'$ region centered on the radio galaxy was used for global temperature and abundance measurements. The surface brightness profiles shown in Figures 5 and 6 are taken from the two sectors.

(A color version of this figure is available in the online journal.)

Thus, we consider this possibility to be unlikely. Following the analysis of Markevitch & Vikhlinin (2007) below, we determine the temperature and pressure across the discontinuity to evaluate which of the other two scenarios, sloshing or supersonic inflation of radio lobes, is more plausible.

We fitted absorbed APEC models to three annuli in two sectors (shown in Figure 4) centered on 3C 288. The vertex of the annuli was fixed at the nucleus, but the binning of the annuli was adjusted, so that the radius of curvature of the second and third annular bins in each fit matches that of the associated discontinuity (i.e., we created the bins so that two annuli were interior and one annulus was exterior to the discontinuity). The goal of this spectral fitting was to determine whether the gas temperature interior to the discontinuities was hotter or cooler than the exterior gas temperature. Only the temperatures and normalizations were free parameters in these fits. The elemental abundance was frozen at the best-fit value determined in the global fits ($Z = 0.73$). Plots of the temperature profiles for the two different sectors, one between position angle (P.A.) = $30°$ and P.A. = $130°$ and another between P.A. = $180°$ and P.A. = $260°$, as a function of radius from the phase center (position of the host galaxy) are shown in Figures 5(c) and 6(c). We find no significant jump in the projected temperature across either discontinuity within 90% error uncertainties of $\Delta T / T \sim 37\%$.

We deprojected the surface brightness profiles (using the best-fit gas temperature derived above) to determine the density and pressure as a function of the distance from the nucleus. Figure 4 shows the ACIS-S image of the central region, with prominent, sharp edges in X-ray brightness at distances from the nucleus of 53.3 kpc ($14''\!.2$) and 91.1 kpc ($24''\!.4$) along the eastern and the southwestern directions, respectively. We model each of these surface brightness discontinuities with a broken power-law density model. We fitted the surface brightness across the discontinuity in the sectors shown in Figure 4 in the energy range 0.5–5.0 keV. The deprojected density and pressure profiles between $30°$ and $130°$ (eastern direction) and between

$180°$ and $260°$ (southwestern direction) as a function of the distance from the cluster center are shown in Figures 5 and 6, panels (b) and (d), respectively. Both brightness profiles have a characteristic shape corresponding to a projection of an abrupt, spherical (within a certain sector) jump in the gas density. Best-fit radial density models of such a shape are shown in panel (b), and their projections are overlaid on the data in panel (a) of Figures 5 and 6. From the amplitude of the best-fitting surface brightness model, we derived a density jump of $1.48^{+0.28}_{-0.24}$ for the eastern discontinuity and $1.75^{+0.68}_{-0.39}$ for the southwestern discontinuity. The confidence ranges for the density jumps were computed from the extremes of the 90% confidence ranges for the best-fitting surface brightness model. As confirmation, the density profile that is derived from the isothermal, azimuthally symmetric surface brightness profile is broadly consistent with the deprojections of the broken power-law models.

To minimize projection effects, we would like to measure the deprojected temperature profile across the jumps; however, the limited number of photons simply does not permit this, although the lack of temperature variation suggests that projection effects are probably not large. Instead, we used the extracted spectra from two large regions for each front for the subsequent analysis: one for the bright side of the front (inside or post-shock) and the other for the faint side of the front (outside or pre-shock). For the eastern jump, we measured a temperature of $2.88^{+1.00}_{-0.66}$ keV inside the jump and $3.46^{+0.86}_{-0.53}$ keV outside the jump, and for the southwestern jump, we measured a temperature of $3.99^{+2.72}_{-1.03}$ keV inside the jump and $3.61^{+1.92}_{-0.94}$ keV outside the jump. The temperature ratios for the two discontinuities are $0.83^{+0.36}_{-0.23}$ and $1.11^{+0.96}_{-0.41}$ for the eastern jump and the southwestern jump, respectively. These uncertainties are at 90% confidence.

4. INTERPRETATION

4.1. Are the Discontinuities Shock Fronts or "Sloshing"?

There are at least two possible explanations for the surface brightness discontinuities: they could be shocks in the gas due to the supersonic inflation of the radio lobes, or they could be contact discontinuities created by non-hydrostatic motions of the gas core due to a recent merger (i.e., "sloshing"). Unfortunately, the quality of the data is not sufficient for us to make a definitive statement about whether these discontinuities are shocks or sloshing. The temperature of the cluster is sufficiently hot (~ 3 keV) that the cluster temperature is not well constrained with less than several thousand counts per spectrum. We favor the shock model, as described below, but arguments can be made for either scenario. We describe some of the implications of both models. Note that our conclusions about the overall energetics of the radio galaxy are not significantly different under the two scenarios. More explicitly, the estimated energy of the outburst is only tens of percent larger for the shock scenario than the subsonic inflation scenario.

4.2. Supersonic Inflation of the Radio Lobes

Several lines of evidence suggest that the discontinuities are shocks, including the relative symmetry of the discontinuities around the nucleus which are not typically seen in sloshing cores, the lack of cool gas in the cluster core, the lack of any evidence of a recent merger in the *Hubble Space Telescope* (*HST*) image of the host galaxy (de Koff et al. 1996), the lack of any evidence of merging on larger scales, and the transformational morphology of the radio source from FR II to FR I
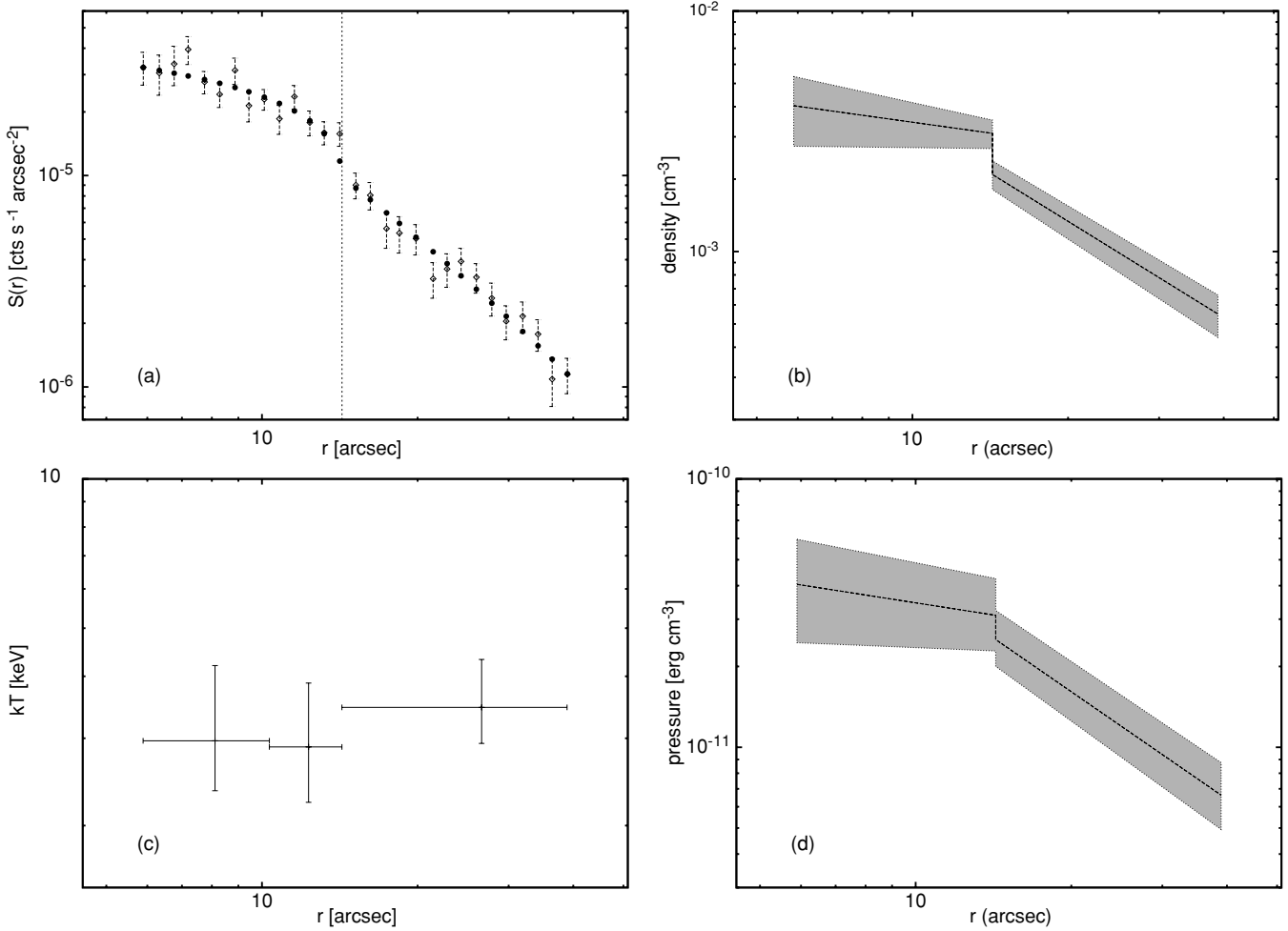
Figure 5. Shock in 3C 288 showing the eastern edge (sector between P.A. = 30° and P.A. = 130°). Panel (a) shows X-ray surface brightness profile. The filled circles are the model values that correspond to the best-fit gas density model shown in panel (b). Panel (c) shows the temperature profile. Panel (d) shows the pressure profile obtained from the temperatures on either side of the edge and density profile. Error bars are 90%; the vertical dashed line in panel (a) shows the position of the density jump.

suggesting that it is strongly interacting with its environment. If these features are shocks, we can estimate the expansion velocity of the radio lobes, total power of the outburst, etc., to constrain the impact the effect of this outburst would have on the surrounding gas. These conclusions could be definitively confirmed (or refuted) with a deeper *Chandra* or *XMM-Newton* observation.

We use the example of M87 to provide a nearby analogy to interpret the features seen in the 3C 288 cluster gas. M87 is the dominant central galaxy in the Virgo cluster showing remarkable morphological details in both the X-ray and the radio (Owen et al. 2000; Hines et al. 1989; Forman et al. 2005). Radio observations show evidence of two distinct nuclear outbursts, and X-ray observations show at least two sets of surface brightness discontinuities in the gas indicative of shocks (Forman et al. 2007). 3C 288 shows a signature of a shock, two regions of enhanced pressure, at a radius of 53.3 kpc on the east and 91.1 kpc on the southwest, similar to M87.

If these features are indeed shocks, the post-shock gas temperature and density will be higher than the pre-shock values in a narrow region behind the shock. With the existing data, we cannot determine the gas temperature profiles across the discontinuities with sufficient accuracy to confirm that they are shocks. Panel (c) in both Figures 5 and 6 shows

the gas temperature profiles across the edges. For a shock discontinuity, the Rankine–Hugoniot jump conditions directly relate the gas density jump, $r \simeq \rho_{shock}/\rho_0$, and the temperature jump, $t \simeq T_{shock}/T_0$, where subscripts "0" and "shock" denote quantities before and after the shock. The Mach number of the shock $M \equiv v/c_s$, where c_s is the velocity of the sound in the pre-shock and v is the velocity of the gas with respect to the plane of the shock (e.g., Landau & Lifshitz 1989). Using the above density jumps, the Mach number is $M \equiv 1.33^{+0.15}_{-0.12}$ and $1.53^{+0.37}_{-0.21}$, respectively, for the eastern and southwestern surface brightness discontinuities. From these density jumps, we predict temperature jumps $T_{shock}/T_0 \equiv 1.32^{+0.38}_{-0.12}$ and $1.52^{+1.16}_{-0.66}$, respectively, for the eastern and southwestern wedges, which are consistent, within error bars, with our measured temperatures. The pressure is discontinuous at the shock front as shown in Figures 5(d) and 6(d) for the eastern and southwestern shocks, respectively.

4.2.1. Merging and "Sloshing"

"Sloshing" of the dense cluster gas core is the term used to describe the non-hydrostatic gas motions induced by a recent merger. When a cluster undergoes a perturbation to its gravitational potential caused by another infalling group or cluster, the gas core lags behind the cluster potential minimum,
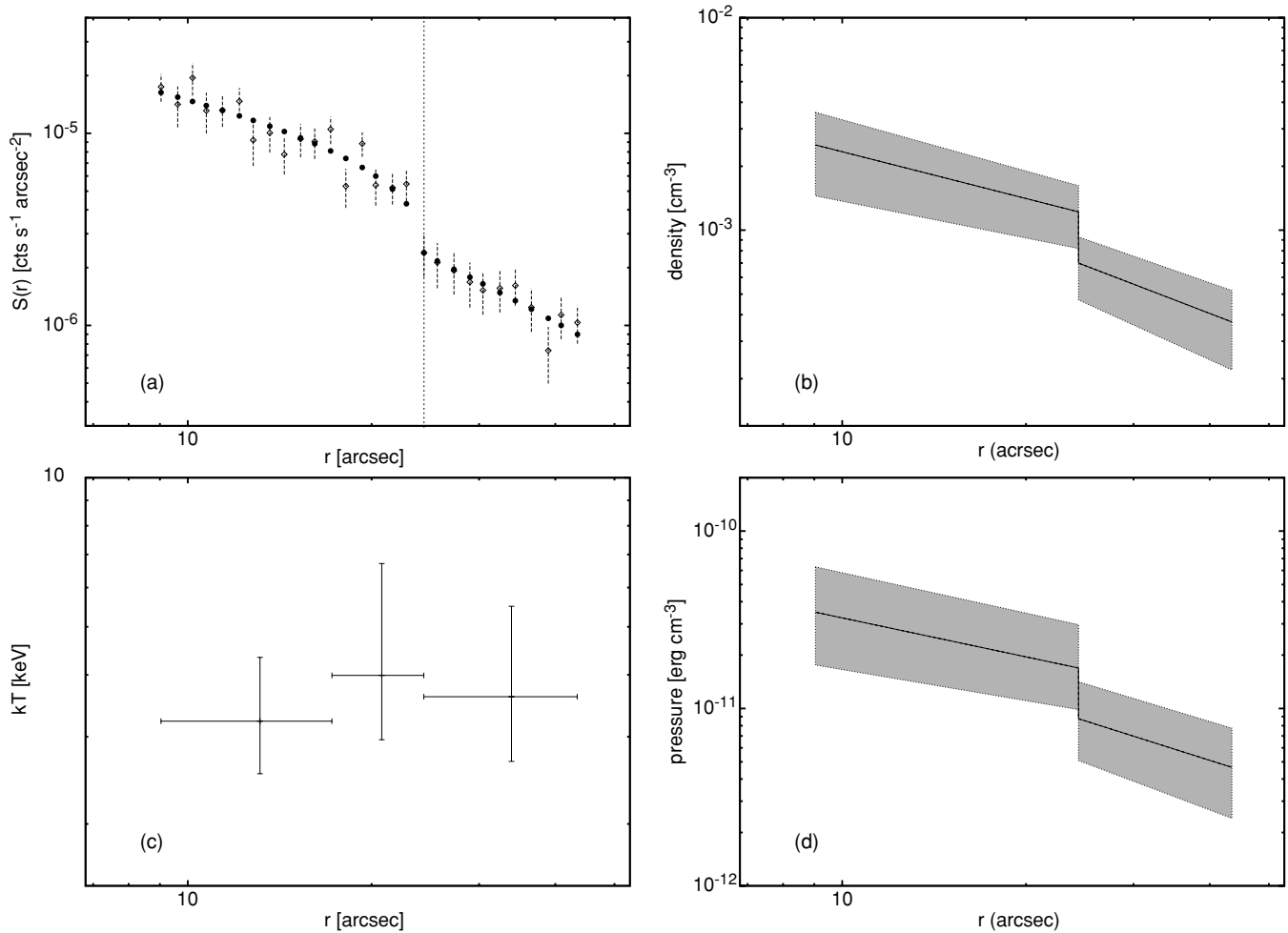
Figure 6. X-ray properties in the southwestern edge (sector between P.A. = 180° and P.A. = 260°). Panel (a) shows X-ray surface brightness profile. The filled circles are the model values that correspond to the best-fit gas density model shown in panel (b). Panel (c) shows the temperature profile. Panel (d) shows the pressure profile obtained from the temperatures on either side of the edge and density profile. Error bars are 90%; the vertical dashed line in panel (a) shows the position of the density jump.

as they both move toward the perturbing object. As the gas core falls back onto the potential minimum, it overshoots it and begins to oscillate. With each oscillation, the gas core is moving against its own trailing gas, producing an "edge" in the X-ray brightness which expands out from the cluster. This sequence of events is described in more detail in Ascasibar & Markevitch (2006) and Markevitch et al. (2001). The continued oscillation of the core gas about the potential minimum produces a succession of radially propagating cold fronts, manifested as concentric edges in the surface brightness distribution. These fronts may form a spiral structure when the sloshing direction is near the plane of the sky and the merger has a non-zero angular momentum (Ascasibar & Markevitch 2006).

The observational features of a cold front are a large temperature jump across the discontinuity (the colder gas is closer to the nucleus) with no discontinuity in pressure. The gas density, and therefore surface brightness, also generally forms a spiral pattern. If we assume that the pressure is continuous across the discontinuity, the temperature jumps should be by factors of $0.67^{+0.13}_{-0.11}$ and $0.57^{+0.22}_{-0.13}$, respectively, based on the derived density jumps for the eastern and the southwestern surface brightness discontinuity. These jumps are well within the uncertainties shown in Figures 5 and 6. If we assume that we are viewing an advanced stage of gas sloshing, the two discon-

tinuities possibly form a clockwise spiral pattern around the core of the cluster because the southwestern discontinuity is farther than the eastern discontinuity from the core. In much better exposed *Chandra* observations of "sloshing," however, the discontinuity is most prominent in one small sector, not equally visible in two nearly opposite directions (Johnson et al. 2010)

To our knowledge, there has been no comprehensive study of individual galaxies of this cluster or measurement of their velocity dispersion. The nearest galaxy to the cluster center detected in the Sloan Digital Sky Survey, SDSS J133850.88+385216.0 ($z = 0.2442$), at a projected distance of ∼0.3 Mpc (1′.131; SDSS DR7; Abazajian et al. (2009)), has no gas associated with it in the *Chandra* image. Additionally, there is no clear pattern of spiral structure in the core, only an offset in the positions of the discontinuities. However, the relatively low quality of the data makes a quantitative statement impossible. We conclude that the only compelling argument to support the sloshing hypothesis is the vague similarity of the discontinuities seen in 3C 288 with other "sloshing" systems, and as described above there are several lines of evidence to suggest they are shocks. A much deeper *Chandra* observation and/or a systematic study of the member galaxies of this cluster would provide a definitive answer.

4.3. Nuclear Outburst

If the surface brightness discontinuities in 3C 288 are shocks, we can estimate (1) the total energy and the age of the outburst, (2) the amount of mass accreted by the central SMBH, and (3) make a strong statement about the effects of outbursts on suppression of the formation of large amounts of cool gas. The total thermal energy of the gas within the core radius of the beta model is $\sim 2.0 \times 10^{60}$ erg. This approach underestimates the true energy because the shock front extends considerably further to the east and southwest, implying a faster, stronger shock, encompassing a greater volume in those directions. However, the value of 2.0×10^{60} erg provides a conservative estimate of the thermal energy of the gas. We estimate the mechanical energy of the outburst by two methods. First, assuming that the bubbles inflated adiabatically, the total bubble enthalpy is $\sim 9.0 \times 10^{59}$ erg. Only 25% of this ($\sim 2.3 \times 10^{59}$ erg) has gone to heat the gas. We have assumed an enthalpy of $4pV$ for each lobe (i.e., $\gamma = 4/3$), and that the lobes can be modeled as cylinders in the plane of the sky (Rafferty et al. 2006). This is the minimum energy of inflation. If the inflation were in fact supersonic, the energy imparted to the gas could be considerably larger. The minimum mean mechanical power of the jet is then $P_{\rm jet} = 6.1 \times 10^{44}$ erg s^{-1} if we assume the bubbles are buoyantly evolving with a mean speed of $0.5c_s$ (Churazov et al. 2001).

We next compute the energy of the outburst assuming that the shock is caused by an isotropic point explosion. We model the shock as a one-dimensional point release of energy into a β-model atmosphere. The parameters of the model, including the energy and age of the burst, are adjusted to fit the observed surface brightness profile. This model has been used to constrain the shock parameters for NGC 4636 and other nuclear outbursts (Baldi et al. 2009). First, for the eastern shock, we fit the shock model to the surface brightness profile, finding that the shock energy is 4.7×10^{59} erg and the shock age is $\sim 3 \times 10^7$ yr. The latter is better determined, since it depends largely on the shock radius and its current speed. Second, for the southwestern shock, a similar analysis yields a shock energy of 7.7×10^{59} erg and a shock age of $\sim 4 \times 10^7$ yr. The two ages are fairly similar and this suggests that there is some asymmetry in the pressure profile. It is conceivable that the shocks arise from two different outbursts. If the shocks are part of a front produced by a single outburst, the total energy would lie (roughly) between these two values, or $\sim 6.2 \times 10^{59}$ erg, and similarly the shock age would be $\sim 3.5 \times 10^7$ yr.

The mass of the central SMBH can be estimated from the $K-z$ data for the 3CRR sample (Willott et al. 2003) and is $\sim 4.0 \times 10^9 \ M_\odot$ (Hardcastle et al. 2007; Marconi & Hunt 2003). Assuming the outburst was powered by the gravitational binding energy released by accretion, and adopting a mass–energy conversion efficiency $\epsilon = 0.1$ and a total outburst energy of between $\sim 0.9 \times 10^{60}$ erg ($= 4pV$) and 1.3×10^{60} erg ($= 3pV +$ shock-outburst-energy), we find that under these assumptions the black hole grew by

$$\Delta M_{\rm BH} = \frac{(1-\epsilon)}{\epsilon} \frac{E}{c^2} = \sim 10^7 M_\odot.$$

Here, $\Delta M_{\rm BH}$ accounts for the lost binding energy and E is the total energy output in mechanical and radiative forms. We ignore radiation because it accounts for a negligible fraction of the current power output. This growth in mass corresponds to an average growth rate of $0.3 \ M_\odot$ yr^{-1} over the past $\sim 3.5 \times 10^7$ yr. Thus, the current outburst is a small ($<1\%$) contribution to the mass of the central SMBH.

Can Bondi accretion of the ICM account for the mechanical power of the outburst (Allen et al. 2006)? It is in principle straightforward to regulate in the context of feedback models and cooling flows (Nulsen & Fabian 2000; Churazov et al. 2002; Sijacki et al. 2007; Somerville et al. 2008; McNamara et al. 2009) and the X-ray atmosphere provides a steady supply of fuel. In relatively low power radio galaxies hosted by giant ellipticals, Bondi accretion has been shown to be energetically feasible in the sense that hot atmospheres probably have a sufficient gas density to supply the mass required to account for the observed jet powers (Di Matteo et al. 2000; Allen et al. 2006; Rafferty et al. 2006; Hardcastle et al. 2009; McNamara et al. 2009).

The average gas density and temperature in the inner $3\farcs2$ (12 kpc) of 3C 288's hot halo are $n_e = 2.3 \times 10^{-2}$ cm^3 and $2.9^{-0.2}_{+0.2}$ keV, respectively. Using the black hole mass of $M_{\rm BH} = 4.0 \times 10^9 \ M_\odot$ (see above), we find a Bondi accretion rate of

$$\dot{M}_{\rm B} = 0.012 \left(\frac{n_e}{0.13}\right) \left(\frac{kT}{2.5}\right)^{-3/2} \left(\frac{M_{\rm BH}}{10^9}\right)^2$$
$$= 2.7 \times 10^{-2} \ M_\odot \ {\rm yr}^{-1}.$$

This value lies roughly an order of magnitude below the $\dot{M} = 0.3 \ M_\odot$ yr^{-1} required to power the current outburst and taken at face value suggests that the current outburst cannot be powered by Bondi accretion of hot cluster medium. We caution however that this result relies on an extrapolation of the temperature and density profile into the core. *Chandra*'s resolution is not sufficient to probe the gas on scales of kiloparsec, and even a modest increase in density and decrease in temperature of the gas on these spatial scales could easily balance the Bondi accretion rate with the mechanical power of the outburst. For example, the gas in the bright cluster galaxies of hot, non-cool core clusters such as Coma is denser and cooler than that of the ambient ICM (Vikhlinin et al. 2001a). The fact that the shock is detached from the lobes, that no X-ray emission is detectable from the central AGN, and that the radio galaxy may be transitioning from FR II to FR I all support the idea that inflation of the lobes has slowed perhaps due to the energy supply to the jet being greatly reduced or cut off. Therefore, it is not surprising that energy released due to the Bondi accretion is currently far less than the mechanical power of the outburst, if the AGN power has recently dropped significantly. Alternatively, it is possible that the current outburst was fueled by accretion of cold gas from, for example, a dusty disk. Such accretion is commonly seen in nearby FR IIs such as 3C 33 (Kraft et al. 2007). There is no evidence of a dusty disk in the *HST* image (de Koff et al. 1996), so it is not clear where this cold gas would originate. Hence, in short, it is plausible for the Bondi accretion to power the current outburst and cold gas could come from a minor merger, but the existing data are of insufficient quality to make a definitive statement.

The estimated energy of the shock is roughly twice the value of the minimum pV work done by the inflation of the lobes, thus demonstrating that supersonic inflation of the lobes can play a key role in the energy balance of cool core clusters. The shock energy is also a significant fraction ($\sim 30\%$) of the total thermal energy of the gas within the radius of the shock. This possibly suggests that the temperature and thermal energy of the gas in the core prior to the inflation of the radio lobes were at least 30% lower. We conclude that we are most likely witnessing AGN feedback in action, and that the outburst, which may have been fueled by Bondi accretion of cooling gas at the cluster center, has likely puffed up the cluster cool core to offset radiative losses.

4.4. Internal Pressure of the Radio Lobes

Finally, we use the measured pressure profile of the gas to determine whether the lobes are at or near equipartition. To estimate the equipartition magnetic field strength, B_{eq}, in the lobes, we make the conventional assumptions that all relevant features are cylinders with depths equal to their radius on the plane of the sky, that the radio spectra are power laws from 10 MHz to 100 GHz, that the filling factor of the emission is unity, and that equal energies reside in the heavy particles and the relativistic electrons. With these assumptions, B_{eq} is ∼50 μG over the lobes, consistent with Bridle et al. (1989), and hence, the equipartition pressure is ∼7.7×10^{-11} dyn cm^{-2}. Using the best-fit models of the β profile, we estimate the thermal gas pressure at the approximate position of the lobes to be ∼1.1×10^{-10} dyn cm^{-2}. Thus, for the case of this FR I/FR II transitional object, the equipartition pressure of the lobe is roughly equal to that of the ambient pressure given the uncertainties of roughly 50%. The result does not change even if we assume that the lobes of 3C 288 do not contain an energetically dominant proton population. This suggests that this "transitional" object is, at least in this regard, more similar to the FR II radio galaxies than the FR Is. It is typically found that the equipartition pressures of lobes in FR I radio galaxies are orders of magnitude less than the ambient gas, while the $P_{eq} \sim P_{gas}$ for FR IIs (Croston et al. 2005, 2008).

5. CONCLUSIONS

3C 288 and its gaseous environment provide a laboratory at moderate redshift for investigating the interaction between an outburst from an SMBH and the surrounding cluster medium. Using the 42 ks *Chandra* observations of 3C 288, we deduce the following.

1. We detect two surface brightness discontinuities in the gas at projected distances of 53.3 (eastern) and 91.1 kpc (southwestern) from the nucleus, which we attribute to shocks from the supersonic inflation of radio lobes.
2. Under the assumption that the discontinuities are shocks, the gas density jumps ($\rho_{shock}/\rho_0 \approx 1.48^{+0.28}_{-0.24}$ and $\rho_{shock}/\rho_0 \approx 1.75^{+0.68}_{-0.39}$, respectively, with 90% uncertainties for the eastern and southwestern shocks) yield shock Mach numbers, $1.33^{+0.15}_{-0.12}$ and $1.53^{+0.37}_{-0.21}$, respectively, for the eastern and southwestern shocks, characteristic of a classical shock in a gas with $\gamma = 5/3$. The data are not of sufficient quality to detect the expected jump in temperature at the discontinuity (T_{shock}/T_0).
3. We measure the energy and age of the shocks to be ∼1.6×10^{60} erg and 3.5×10^7 yr, respectively.
4. The radio lobes are not far from equipartition.

Chandra has detected shocks from the supersonic inflation of radio lobes in nearly two dozen galaxies, groups, and clusters, but the discovery of shocks reported here is the most distant reported to date. It is now clear that feedback between cooling gas and the central SMBH plays a critical role in the evolution of early-type galaxies and the central regions of groups and clusters. These outbursts probably suppress star formation in massive galaxies and are the origin of the exponential decay in the galaxy mass function at large masses. A well-selected *Chandra* survey could detect a significant number of examples of such phenomena in massive systems out to redshift ∼0.5. The look-back time to 3C 288 is only about 15% of the Hubble time, so even this observation has not yet begun to directly study the role of shock-heating in the epoch of cluster formation ($z \sim 1$ and beyond). Given the relative faintness and rarity of even the most massive clusters beyond $z \sim 0.5$, it would be difficult to make a detailed study with *Chandra* at and beyond the redshift at which clusters are forming.

REFERENCES

Abazajian, K. N., et al. 2009, ApJS, 182, 543
Allen, S., Dunn, R. J. H., Fabian, A. C., Taylor, G. B., & Reynolds, C. S. 2006, MNRAS, 372, 21
Anders, E., & Grevesse, N. 1989, Geochim. Cosmochim. Acta, 53, 197
Arnaud, K. A. 1996, in ASP Conf. Ser. 101, Astronomical Data Analysis Software and Systems V, ed. H. J. George & B. Jeannette (San Francisco, CA: ASP), 17
Ascasibar, Y., & Markevitch, M. 2006, ApJ, 650, 102
Baldi, A., Forman, W., Jones, C., Kraft, R., Nulsen, P., Churazov, E., David, L., & Giacintucci, S. 2009, ApJ, 707, 1034
Bridle, A. H., Fomalont, E. B., Byrd, G. G., & Valtonen, M. J. 1989, AJ, 97, 674
Burns, J. O., O'Dea, C. P., Gregory, S. A., & Balonek, T. J. 1986, ApJ, 307, 73
Churazov, E., Brüggen, M., Kaiser, C. R., Böhringer, H., & Forman, W. 2001, ApJ, 554, 261
Churazov, E., Sunyaev, R., Forman, W., & Böhringer, H. 2002, MNRAS, 332, 729
Croston, J. A., Hardcastle, M. J., Harris, D. E., Belsole, E., Birkinshaw, M., & Worrall, D. M. 2005, ApJ, 626, 733
Croston, J. H., Hardcastle, M. J., Birkinshaw, M., Worrall, D. M., & Laing, R. A. 2008, MNRAS, 386, 1709
David, L. P., Jones, C., Forman, W., Vargas, I. M., & Nulsen, P. 2006, ApJ, 653, 207
de Koff, S., Baum, S. A., Sparks, W. B., Biretta, J., Golombek, D., Macchetto, F., McCarthy, P., & Miley, G. K. 1996, ApJS, 107, 621
Dickey, J. M., & Lockman, F. J. 1990, ARA&A, 28, 215
Di Matteo, T., Quataert, E., Allen, S. W., Narayan, R., & Fabian, A. C. 2000, MNRAS, 311, 507
Ellingson, E., Green, R. F., & Yee, H. K. C. 1991a, ApJS, 76, 455
Ellingson, E., Yee, H. K. C., & Green, R. F. 1991b, ApJ, 371, 49
Ellingson, E., Yee, H. K. C., & Green, R. F. 1991c, ApJ, 378, 476
Erlund, M. C., Fabian, A. C., Blundell, K. M., Moss, C., & Ballantyne, D. R. 2007, MNRAS, 379, 498
Fanaroff, B. L., & Riley, J. M. 1974, MNRAS, 167, P31
Finoguenov, A., Briel, U. G., & Henry, J. P. 2003, A&A, 410, 777
Forman, W. R., et al. 2005, ApJ, 635, 894
Forman, W. R., et al. 2007, ApJ, 665, 1057
Goodson, R. E., Palimaka, J. J., & Bridle, A. H. 1979, AJ, 84, 1111
Hardcastle, M. J., Evans, D. A., & Croston, J. H. 2007, MNRAS, 376, 1849
Hardcastle, M. J., Evans, D. A., & Croston, J. H. 2009, MNRAS, 396, 1926
Hardcastle, M. J., Worrall, D. M., Birkinshaw, M., Laing, R. A., & Bridle, A. H. 2002, MNRAS, 334, 182
Harvanek, M., Ellingson, E., Stocke, J. T., & Rhee, G. 2001, AJ, 122, 2874
Harvanek, M., & Stocke, J. T. 2002, AJ, 124, 1239
Hines, D. C., Eilek, J. A., & Owen, F. N. 1989, ApJ, 347, 713
Isobe, N., Makishima, K., Tashiro, M., & Hong, S. 2005, ApJ, 632, 781

Johnson, R. E., Markevitch2, M., Wegner, G. A., Jones, C., & Forman, W. R. 2010, ApJ, 710, 1776

Kraft, R. P., Azcona, J., Forman, W. R., Hardcastle, M. J., Jones, C., & Murray, S. S. 2006, ApJ, 639, 753

Kraft, R. P., Birkinshaw, M., Hardcastle, M. J., Evans, D. A., Croston, J. H., Worrall, D. M., & Murray, S. S. 2007, ApJ, 659, 1008

Laing, R. A., & Peacock, J. A. 1980, MNRAS, 190, 903

Laing, R. A., Riley, J. M., & Longair, M. S. 1983, MNRAS, 204, L151

Landau, L. D., & Lifshitz, E. M. 1989, Fluid Mechanics (2nd ed.; Butterworth and Heineman)

Marconi, A., & Hunt, L. K. 2003, ApJ, 589, L21

Markevitch, M. 1998, ApJ, 504, 27

Markevitch, M., & Vikhlinin, A. 2007, Phys. Rep., 443, 1

Markevitch, M., Vikhlinin, A., & Mazzotta, P. 2001, ApJ, 562, L153

McNamara, B. R., Kazemzadeh, F., Rafferty, D. A., Bîrzan, L., Nulsen, P. E. J., Kirkpatrick, C. C., & Wise, M. W. 2009, ApJ, 698, 594

McNamara, B. R., & Nulsen, P. E. J. 2007, ARA&A, 45, 117

McNamara, B. R., Nulsen, P. E. J., Wise, M. W., Rafferty, D. A., Carilli, C., Sarazin, C. L., & Blanton, E. L. 2005, Nature, 433, 35

Nulsen, P. E. J., & Fabian, A. C. 2000, MNRAS, 311, 346

Nulsen, P. E. J., McNamara, B. R., Wise, M. W., & David, L. P. 2005, ApJ, 628, 629

Owen, F. N., Eilek, J. A., & Kassim, N. E. 2000, ApJ, 543, 611

Owers, M. S., Nulsen, P. E. J., Couch, W. J., & Markevitch, M. 2009, ApJ, 704, 1349

Peterson, J. R., & Fabian, A. C. 2006, Phys. Rep., 427, 1

Rafferty, D. A., McNamara, B. R., Nulsen, P. E. J., & Wise, M. W. 2006, ApJ, 652, 1216

Sambruna, R. M., Gliozzi, M., Donato, D., Tavecchio, F., Cheung, C. C., & Mushotzky, R. F. 2004, A&A, 414, 885

Sarazin, C. L., & Lieu, R. 1998, ApJ, 494, L177

Sijacki, D., Springel, V., Di Matteo, T., & Hernquist, L. 2007, MNRAS, 380, 877

Smith, D. A., Wilson, A. S., Arnaud, K. A., Terashima, Y., & Young, A. J. 2002, ApJ, 565, 195

Somerville, R. S., Hopkins, P. F., Cox, T. J., Robertson, B. E., & Hernquist, L. 2008, MNRAS, 391, 481

Spergel, D. N., et al. 2007, ApJS, 170, 377

Vikhlinin, A., Markevitch, M., Forman, W., & Jones, C. 2001a, ApJ, 555, L87

Vikhlinin, A., Markevitch, M., & Murray, S. S. 2001b, ApJ, 551, 160

Willott, C. J., Rawlings, S., Jarvis, M. J., & Blundell, K. M. 2003, MNRAS, 339, 173

Wyndham, J. D. 1966, ApJ, 144, 459